

The Behrens–Fisher problem revisited

Nagananda K G and Jong Sung Kim*

Abstract

We revisit the two-sample Behrens–Fisher problem—testing equality of means when two normal populations have unequal, unknown variances—and derive a compact expression for the null distribution of the classical test statistic. The key step is a Mellin–Barnes factorization that decouples the square root of a weighted sum of independent chi-square variates, thereby collapsing a challenging two-dimensional integral to a tractable single-contour integral. Closing the contour yields a residue series that terminates whenever either sample’s degrees of freedom is odd. A complementary Euler–Beta reduction identifies the density as a Gauss hypergeometric function with explicit parameters, yielding a numerically stable form that recovers Student’s t under equal variances. Ramanujan’s master theorem supplies exact inverse-power tail coefficients, which bound Lugannani–Rice saddle-point approximation errors and support reliable tail analyses. Our result subsumes the hypergeometric density derived by Nel et al., and extends it with a concise cdf and analytic tail expansions; their algebraic special cases coincide with our truncated residue series. Using our derived expressions, we tabulate exact two-sided critical values over a broad grid of sample sizes and variance ratios that reveal the parameter surface on which the well-known Welch’s approximation switches from conservative to liberal, quantifying its maximum size distortion.

Keywords: Mellin–Barnes integral; hypergeometric functions; Ramanujan’s theorem.

1 Introduction

Consider independent samples $X_1, \dots, X_{n_1} \stackrel{\text{iid}}{\sim} \mathcal{N}(\mu_1, \sigma_1^2)$ and $Y_1, \dots, Y_{n_2} \stackrel{\text{iid}}{\sim} \mathcal{N}(\mu_2, \sigma_2^2)$ from two normal populations. Let $\nu_i = n_i - 1$, $\bar{X} = \frac{1}{n_1} \sum_{i=1}^{n_1} X_i$, $\bar{Y} = \frac{1}{n_2} \sum_{i=1}^{n_2} Y_i$, $S_1^2 = \frac{1}{\nu_1} \sum_{i=1}^{\nu_1} (X_i - \bar{X})^2$, $S_2^2 = \frac{1}{\nu_2} \sum_{i=1}^{\nu_2} (Y_i - \bar{Y})^2$ denote the degrees of freedom, the sample means and the sample variances, respectively, of the two samples. For notational convenience, let $g = \sigma_1^2/n_1$, $h = \sigma_2^2/n_2$ and variance ratio $r = \sigma_1^2/\sigma_2^2$. Following the pioneering work of Behrens [1] and Fisher [2], the problem of testing $H_0: \mu_1 = \mu_2$ with (σ_1^2, σ_2^2) unknown and $\sigma_1^2 \neq \sigma_2^2$ (*i.e.*, $g \neq h$) remains an enduring challenge in mathematical statistics. Although several approximations, modifications and practical procedures have been proposed (for example, [3–15])—including nonparametric versions of the test [16–19]—to the best of our

*The authors are with the Department of Mathematics and Statistics, Portland State University, Portland, OR 97201, USA. E-mail: {nanda, jong}@pdx.edu.

knowledge, no explicit canonical expression for the density function of the Behrens–Fisher statistic

$$T = \frac{\bar{X} - \bar{Y}}{\sqrt{\frac{S_1^2}{n_1} + \frac{S_2^2}{n_2}}} \quad (1)$$

has been established in terms of standard probability distribution functions. The absence of such a representation complicates exact significance evaluation, power calculations, and asymptotic error control—particularly in the small-sample, high-variance-imbalance regimes common in modern experimental design.

Under H_0 , $\bar{X} - \bar{Y} \sim \mathcal{N}(0, g + h)$; $\frac{\nu_1 S_1^2}{\sigma_1^2} \sim \chi_{\nu_1}^2$, $\frac{\nu_2 S_2^2}{\sigma_2^2} \sim \chi_{\nu_2}^2$, and these are independent of \bar{X} and \bar{Y} . The key challenge is that, when forming the ratio for T the denominator involves $\sqrt{S_1^2/n_1 + S_2^2/n_2}$, which is a nonlinear function of two independent χ^2 variables scaled by σ_1^2 and σ_2^2 that are unknown and $\sigma_1^2 \neq \sigma_2^2$. In attempting a closed-form expression for the distribution of T , conditioned on *a priori* knowledge of (σ_1^2, σ_2^2) , we can write

$$T = \frac{\bar{X} - \bar{Y}}{\sqrt{\frac{gW_1}{\nu_1} + \frac{hW_2}{\nu_2}}}, \quad (2)$$

where $W_i = \nu_i S_i^2 / \sigma_i^2$, $i = 1, 2$. Under H_0 , we have $W_i \sim \chi_{\nu_i}^2$, $i = 1, 2$. This yields

$$T | \sigma_1^2, \sigma_2^2 \sim \frac{\mathcal{N}(0, g + h)}{\sqrt{\frac{gW_1}{\nu_1} + \frac{hW_2}{\nu_2}}}. \quad (3)$$

When $\sigma_1^2 = \sigma_2^2 = \sigma^2$, and σ^2 unknown, we have the likelihood ratio statistic

$$T | \sigma^2 \sim \frac{(\bar{X} - \bar{Y})}{\sqrt{S_p^2 \left(\frac{1}{n_1} + \frac{1}{n_2} \right)}}, \quad (4)$$

where the pooled variance estimate

$$S_p^2 = \frac{1}{\nu_1 + \nu_2} \left(\sum_{j=1}^{\nu_1} (X_j - \bar{X})^2 + \sum_{j=1}^{\nu_2} (Y_j - \bar{Y})^2 \right). \quad (5)$$

This implies $T | \sigma^2 \sim t_{\nu_1 + \nu_2}$, the Student’s two-sample t -test following a t -distribution with $(\nu_1 + \nu_2)$ degrees of freedom (see [20, Exercise 8.41]). However, when $\sigma_1^2 \neq \sigma_2^2$ and (σ_1^2, σ_2^2) unknown, no such simplification—including using the pooled variance estimate S_p^2 —is possible (see [20, Exercise 8.42]). The distribution of

$$T = \frac{\bar{X} - \bar{Y}}{\sqrt{\frac{gW_1}{\nu_1} + \frac{hW_2}{\nu_2}}} \quad (6)$$

would require integrating over the joint density of (W_1, W_2) :

$$f_T(t) = \int_0^\infty \int_0^\infty f_{T|W_1, W_2}(t) f_{W_1}(w_1) f_{W_2}(w_2) dw_1 dw_2, \quad (7)$$

where each of $f_{W_1}(w_1)$ and $f_{W_2}(w_2)$ is the pdf of a χ^2 distribution. The conditional density $f_{T|W_1, W_2}(t)$ is normal with a variance that depends on w_1 and w_2 . Thus, we have

$$f_T(t) = \int_0^\infty \int_0^\infty \frac{\sqrt{gw_1/\nu_1 + hw_2/\nu_2}}{\sqrt{2\pi(g+h)}} \exp\left(-\frac{t^2(gw_1/\nu_1 + hw_2/\nu_2)}{2(g+h)}\right) f_{W_1}(w_1) f_{W_2}(w_2) dw_1 dw_2. \quad (8)$$

Efforts to solve (8) does not yield a closed-form expression in terms of elementary distributions. This complexity is the centerpiece of the Behrens–Fisher problem: lifting the equal-variance assumption transforms the otherwise straightforward two-sample t -test into a setting where no exact, closed-form distribution is available in elementary terms. In addressing this problem, Welch [21] employed the approximation developed by Satterthwaite [22] to replace the unknown degrees of freedom with a carefully crafted estimate,

$$\hat{\nu} \approx \frac{\left(\frac{S_1^2}{n_1} + \frac{S_2^2}{n_2}\right)^2}{\left[\frac{S_1^4}{n_1^2 \nu_1} + \frac{S_2^4}{n_2^2 \nu_2}\right]}, \quad (9)$$

thereby yielding $T \stackrel{\text{approx}}{\sim} t_{\hat{\nu}}$ with $\hat{\nu}$ degrees of freedom. Welch’s test controls the Type I error rate, does not require equal variances and is more robust than the classic pooled-variance t -test (see [20, Chapter 8]). The Welch–Satterthwaite approximation has been the main workhorse for the Behrens–Fisher problem in practical applications.

We make progress on this problem by deriving an expression for the null distribution of T that is simultaneously compact, rapidly computable and amenable to asymptotic analyses. Leveraging a Mellin–Barnes (MB) contour decomposition [23], we disentangle the square-root coupling $(gW_1/\nu_1 + hW_2/\nu_2)^{1/2}$ between the independent χ^2 -variates W_1 and W_2 . This step collapses the conventional two-dimensional integral representation of the density into a one-dimensional contour integral whose integrand is a product of Gamma functions. Such MB collapses have proved potent in analytic number theory and special-function theory, yet have not previously been applied to the Behrens–Fisher problem. Closing the MB contour on the right yields a hypergeometric-type residue series. The infinite sum thus obtained becomes a finite polynomial-over-rational expression—no tail terms of order $k > \frac{\nu_i-1}{2}$ survive. The series involves the factor $\Gamma\left(\frac{\nu_2}{2} - k + \frac{1}{2}\right)$, $k = 0, 1, \dots$, and if, say, $\nu_2 = 2m + 1$ (*i.e.*, odd) then the argument hits a non-positive integer at $k = m$; the Gamma function is infinite there, but its reciprocal appears in the residue coefficient, giving zero residue for every $k > m$. Hence, only the first $m + 1$ terms remain and the sum terminates. An analogous cut-off occurs when ν_1 is odd. This finite-sum phenomenon explains scattered algebraic densities reported in numerical tables from the 1950s (see, for instance, [24, Table 55]) but never formally derived; our terminating series supplies the missing derivation and shows that

every odd ν_i row in the Biometrika tables is the closed residue sum, not a separate special case. For general ν_1, ν_2 , the resulting infinite series converges at a geometric rate controlled by $\min\{g, h\}/(g+h)$, enabling high-precision density evaluations with fewer than ten terms across virtually the entire support.

We complement the residue expansion by an Euler (S, U) –change of variables that separates a radial component $S = gW_1/\nu_1 + hW_2/\nu_2$ and a Beta-distributed mixing fraction U . The integral in U can be performed in a closed form, producing the compact density

$$f_T(t) = C [2/B(t)]^c {}_2F_1\left(c, \frac{\nu_1}{2}; \frac{\nu_1+\nu_2}{2}; -\rho(t)\right), \quad (10)$$

with explicit expressions for C and $B(t)$, where $c = (\nu_1 + \nu_2 + 1)/2$ and $\rho(t) = (g^{-1} - h^{-1})/(h^{-1} + t^2/(g+h))$ and ${}_2F_1$ is Gauss’ hypergeometric function and all parameters are explicit. The expression collapses seamlessly to the Student- $t_{\nu_1+\nu_2-2}$ density when $g = h$ and to a rational function when one variance dominates, integrating disparate corner cases into a coherent framework. While hypergeometric representations have appeared in isolated special-case studies (for instance, [11]), our result is valid for all (n_1, n_2, r) . Its derivation also clarifies structural symmetries—particularly the invariance under $(\nu_1, \nu_2, g, h) \mapsto (\nu_2, \nu_1, h, g)$ —and provides analytic gradients for likelihood-based estimation of variance ratios in random-effect meta-analyses.

The MB contour representation admits two analytically complementary pathways. First, Euler–Beta reduction: by rewriting W_1, W_2 in polar coordinates $S = gW_1/\nu_1 + hW_2/\nu_2, U = gW_1/\nu_1 S$, the inner S –integral is a Gamma integral and the remaining U –integral equals Euler’s Beta integral representation of Gauss’ hypergeometric function [25]. This gives a closed form expression for $f_T(t)$ described in the aforementioned paragraph; the same identity collapses to Student- t when $g = h$. Second, Ramanujan’s master theorem (RMT) [26] transforms the MB integrand into an inverse–Mellin power series, producing an exact tail expansion $f_T(t) = \sum_{m \geq 0} (-1)^m A_m |t|^{-(2m+1)}/m!$ with A_m as closed Gamma products. The remainder after M terms is $O(|t|^{-(2M+3)})$, leading to deterministic error bounds for any truncated series and gives algebraic control unavailable in simulation-based methods. The same cumulant generator feeds the Lugannani–Rice (LR) saddle-point formula $P(T > t) \approx \Phi(-w) + \phi(w)(1/w - 1/u)$ [27], with w, u expressed in cumulants of T . Using RMT coefficients, we prove a uniform remainder $O(|t|^{-4})$ when $|t| < 0.8 \min\{\nu_1, \nu_2\}$ and quantify the accuracy loss in the variance–extreme corners ($|\log_{10} r| > 1$). These three ingredients—Euler–Beta for the bulk, RMT for the far tail, and LR to bridge the regimes—enable fast and accurate evaluation of the density, distribution function and quantiles through closed-form and numerically stable methods, without resort to computationally intensive simulation.

It was first recognized by Nel et al. [28] that the Behrens–Fisher density can be written as a single Gauss hypergeometric function, but they derived the expression only for the univariate case, gave no proof of termination when a degree of freedom is odd, provided neither cumulative distribution function (cdf) nor tail theory, and concluded that their formula was computationally impractical. Our MB treatment reproduces their pdf as one branch of a

richer structure: the residue series shows *why* the hypergeometric terminates when ν_1 or ν_2 is odd, the Euler–Beta route supplies a closed-form cdf (an Appell F_1 integral) for the first time, and Ramanujan’s coefficients turn the putative obstacle of numerical instability into an explicit $|t|^{-(2m+1)}$ tail expansion with deterministic error bounds. On the approximation side, Welch’s $t_{\hat{\nu}}$ statistic replaces the true tail exponent $\nu_1 + \nu_2 + 1$ by a random $\hat{\nu}$; using our exact density we compute critical-value grids that locate the surface where $E[\hat{\nu}] = \nu_1 + \nu_2$ and show that, away from this surface, Welch can be up to 60% liberal or conservative in samples as small as $n_1 = n_2 = 10$. It is also of interest to note that, [9] constructed exact tests, but only supply critical constants—not a symbolic density. Their method does not reveal the algebraic structure (hypergeometric kernel, termination when ν_i is odd, Ramanujan tails) that our MB analysis uncovers. Their exactness is achieved by numerical double integration for every (n_1, n_2, r) . We give an expression that works for all (n_1, n_2, r) in a single expression.

The remainder of the paper is organized as follows. In Section 2, the Mellin–Barnes representation of T is presented. The density function $f_T(t)$ is expressed as a Gauss hypergeometric function ${}_2F_1$ by reducing the 2-D integral to a 1-D integral in Section 3. The tail analyses of $f_T(t)$ using Ramanujan’s master theorem is in Section 4. Some discussions including cdf tables, Lugannani–Rice saddle-points, and comparisons between our work with Welch’s [21] and Nel et al. [28] are provided in Section 5. Section 6 concludes the paper.

2 Mellin–Barnes representation of T

Consider the Behrens–Fisher statistic $T = \frac{\bar{X} - \bar{Y}}{\sqrt{S_1^2/n_1 + S_2^2/n_2}}$ with $\nu_i = n_i - 1$ degrees of freedom, and recall the notation introduced in Section 1: $g = \frac{\sigma_1^2}{n_1}$, $h = \frac{\sigma_2^2}{n_2}$, $W_1 = \frac{\nu_1 S_1^2}{\sigma_1^2}$, $W_2 = \frac{\nu_2 S_2^2}{\sigma_2^2}$. Under $H_0 : \mu_1 = \mu_2$, we have $\bar{X} - \bar{Y} | (\sigma_1^2, \sigma_2^2) \sim \mathcal{N}(0, g + h)$, and this difference is independent of (S_1^2, S_2^2) . Hence, conditional on the random denominator, the statistic T is merely a scaled normal ratio:

$$T | (W_1, W_2) \sim \frac{\mathcal{N}(0, g + h)}{\sqrt{\frac{gW_1}{\nu_1} + \frac{hW_2}{\nu_2}}} \quad (11)$$

with the following pdf:

$$f_{T|W_1, W_2}(t) = \frac{\sqrt{gW_1/\nu_1 + hW_2/\nu_2}}{\sqrt{2\pi}(g + h)} \exp\left[-\frac{t^2}{2(g + h)}(gW_1/\nu_1 + hW_2/\nu_2)\right], \quad (12)$$

where $W_1 \sim \chi_{\nu_1}^2$, $W_2 \sim \chi_{\nu_2}^2$, $W_1 \perp W_2$, so their pdfs are

$$f_{W_i}(w) = \frac{w^{\nu_i/2-1} e^{-w/2}}{2^{\nu_i/2} \Gamma(\nu_i/2)}, \quad w > 0, \quad i = 1, 2. \quad (13)$$

There is no closed-form pdf for the weighted sum $\sqrt{gW_1/\nu_1 + hW_2/\nu_2}$; this is the core obstacle of the Behrens–Fisher problem, so we keep the bivariate (W_1, W_2) pair intact.

Since T depends on (W_1, W_2) only through the scale factor, and because of the aforementioned independence, the unconditional density is

$$\begin{aligned} f_T(t) &= \mathbb{E}_{(W_1, W_2)} [f_{T|W_1, W_2}(t)] \\ &= \int_0^\infty \int_0^\infty \underbrace{\frac{\sqrt{\frac{gw_1}{\nu_1} + \frac{hw_2}{\nu_2}}}{\sqrt{2\pi(g+h)}} \exp\left[-\frac{t^2}{2(g+h)} \left(\frac{gw_1}{\nu_1} + \frac{hw_2}{\nu_2}\right)\right]}_{f_{T|W_1, W_2}(t)} f_{W_1}(w_1) f_{W_2}(w_2) dw_1 dw_2. \end{aligned} \quad (14)$$

Subsequent analytic techniques (MB representation, contour collapse, hypergeometric reduction, saddle-point expansion) on the integral (14) make transparent which pieces are manipulable (Gamma-type factors) and which pieces pose a challenge (the two scale contributions gw_1 and hw_2 inside both the square root and the exponential). The term $\sqrt{(gw_1/\nu_1 + hw_2/\nu_2)}$ in (14) is non-factorizable, but can be linearized by the MB identity

$$(x+y)^\rho = \frac{1}{2\pi i} \int_{c-i\infty}^{c+i\infty} \frac{\Gamma(-s) \Gamma(\rho+s)}{\Gamma(\rho)} x^s y^{\rho-s} ds. \quad (15)$$

Since the integrand is a product of independent Gamma-type factors, $\int_0^\infty w_i \exp[-(\cdot)w_i] dw_i$ is an ordinary Gamma integral; we collapse the double integral to a single complex contour integral. Once in the MB form, closing the contour yields either an explicit convergent series (useful for small and moderate degrees of freedom), or a finite sum if either ν_i is odd, or a one-line hypergeometric function after an Euler– u transformation, paving the way for compact expression for $f_T(t)$. Furthermore, Ramanujan’s master theorem covers the MB integrand’s product of Γ –functions, thereby providing the coefficients in the large– $|t|$ expansion.

2.1 MB expansion of the square-root factor

We now invoke a complex-contour identity to pull apart the term $\sqrt{(gw_1/\nu_1 + hw_2/\nu_2)}$. In (14), the only place where w_1, w_2 are entangled is the square-root factor $\sqrt{(gw_1/\nu_1 + hw_2/\nu_2)}$. Everything else is already factorized: the exponential separates because $\exp[-\alpha(gw_1/\nu_1 + hw_2/\nu_2)] = \exp[-\alpha gw_1/\nu_1] \exp[-\alpha hw_2/\nu_2]$, and each χ^2 density only depends on its own variable. Hence, if we can rewrite $\sqrt{(gw_1/\nu_1 + hw_2/\nu_2)}$ in a form such that the sum/integral factorizes into a product of a w_1 –power and a w_2 –power, the double integral collapses into two independent Gamma integrals. That is exactly what an MB representation does.

For any positive reals $x, y > 0$, any complex exponent ρ , and any vertical contour $\Re s = c$ satisfying $-\Re \rho < c < 0$, the Barnes integral is given by (15). It is simply the inverse Mellin transform of the Beta function $B(-s, \rho+s) = \Gamma(-s)\Gamma(\rho+s)/\Gamma(\rho)$, with the following

pole structure: $\Gamma(-s)$ has simple poles at $s = 0, 1, 2, \dots$; $\Gamma(\rho + s)$ has simple poles at $s = -\rho, -\rho - 1, -\rho - 2, \dots$. Choosing c between those two interlacing ladders guarantees integral convergence. Also, closing the contour to the right (resp. left) picks up the $\Gamma(-s)$ (resp. $\Gamma(\rho + s)$) poles and reproduces the familiar binomial (or inverse-binomial) power series $\sum_{k \geq 0} \binom{\rho}{k} x^k y^{\rho-k}$. Taking the special exponent $\rho = \frac{1}{2}$ gives, for $-\frac{1}{2} < c < 0$,

$$(x + y)^{\frac{1}{2}} = \frac{1}{2\pi i} \int_{c-i\infty}^{c+i\infty} \frac{\Gamma(-s) \Gamma(\frac{1}{2} + s)}{\Gamma(\frac{1}{2})} x^s y^{1/2-s} ds, \quad (16)$$

Since $\Gamma(\frac{1}{2}) = \sqrt{\pi}$, no extra constants appear. Setting $x = gw_1/\nu_1$, $y = hw_2/\nu_2$, $\rho = \frac{1}{2}$ yields

$$\sqrt{(gw_1/\nu_1 + hw_2/\nu_2)} = \frac{1}{2\pi i \sqrt{\pi}} \int_{c-i\infty}^{c+i\infty} \Gamma(-s) \Gamma(\frac{1}{2} + s) \left(\frac{g}{\nu_1}\right)^s w_1^s \left(\frac{h}{\nu_2}\right)^{1/2-s} w_2^{1/2-s} ds. \quad (17)$$

The inseparable factor is now a weighted geometric mean $(g/\nu_1)^s w_1^s (h/\nu_2)^{1/2-s} w_2^{1/2-s}$ multiplied by a pure- s coefficient (the Γ -product). All w_1 -dependence and w_2 -dependence are split into separate powers. This makes the forthcoming integrations elementary.

Since absolutely convergent integrals may be rearranged, we move the MB contour outside:

$$f_T(t) = \frac{1}{2\pi i \sqrt{\pi} \sqrt{2\pi(g+h)}} \int_{c-i\infty}^{c+i\infty} \Gamma(-s) \Gamma(\frac{1}{2} + s) \left(\frac{g}{\nu_1}\right)^s \left(\frac{h}{\nu_2}\right)^{1/2-s} [J_1(s) J_2(s)] ds, \quad (18)$$

with the factorized one-dimensional Gamma integrals

$$J_1(s) = \int_0^\infty w_1^{s+\nu_1/2-1} \exp\left[-\left(\frac{1}{2} + \frac{\alpha g}{\nu_1}\right) w_1\right] dw_1 = \frac{\Gamma(s + \nu_1/2)}{\left(\frac{1}{2} + \frac{\alpha g}{\nu_1}\right)^{s+\nu_1/2}}, \quad (19)$$

$$J_2(s) = \int_0^\infty w_2^{\nu_2/2-s-1/2} \exp\left[-\left(\frac{1}{2} + \frac{\alpha h}{\nu_2}\right) w_2\right] dw_2 = \frac{\Gamma(\nu_2/2 - s + \frac{1}{2})}{\left(\frac{1}{2} + \frac{\alpha h}{\nu_2}\right)^{\nu_2/2-s+1/2}}, \quad (20)$$

where $\alpha = \frac{t^2}{2(g+h)}$. With this development, (18) is precisely the single-contour formula.

Two dimensions have become one; the price is the integral over a vertical line in the complex plane. From here, residue calculus yields an explicit series by closing the contour to the right: poles of $\Gamma(-s)$ at $s = 0, 1, \dots$ give the hypergeometric-type series, which terminates when either ν_1 or ν_2 is odd. Alternatively, before the MB step, one may collapse (w_1, w_2) to (S, U) . But, the MB path is shorter: from (18), shift the contour left, pick the poles of $\Gamma(\frac{1}{2} + s)$, and recognize the resulting Beta function integral as Gauss' hypergeometric, thereby facilitating a compact expression for $f_T(t)$ that becomes apparent in the sequel. More importantly, the

integrand in (18) is exactly of the γ -product type that Ramanujan's master theorem turns into asymptotic series without further work: expand the Γ -ratio around large s to read off the $|t| \rightarrow \infty$ expansion coefficients directly, thereby yielding exact tail coefficients.

The MB approach works for all g, h . While Taylor series in w_1/w_2 converges only when one weight is smaller than the other, the MB integral is valid everywhere. It handles non-integer exponents naturally. In our case, the exponent is $\rho = \frac{1}{2}$; the MB representation is tailor-made for arbitrary complex ρ . Note that, MB aids interfacing with Γ -distributions: χ^2 densities are special cases of Γ -densities. The MB splits $(x + y)^\rho$ into Γ -functions of s times monomials in x and y —perfectly aligned with Γ integrals. Furthermore, the MB integrals provide contour flexibility. We may choose to close left or right, whichever set of poles yields the nicer series (terminating, fastest convergence, *etc*).

2.2 Residue calculus on the MB contour

From the MB expansion, we have

$$f_T(t) = \frac{1}{(2\pi)^2 i \sqrt{\pi(g+h)}} \int_{c-i\infty}^{c+i\infty} \frac{\Psi(s) \left(\frac{g}{\nu_1}\right)^s \left(\frac{h}{\nu_2}\right)^{1/2-s} \Gamma\left(s + \frac{\nu_1}{2}\right) \Gamma\left(\frac{\nu_2}{2} - s + \frac{1}{2}\right)}{\left(\frac{1}{2} + \frac{\alpha g}{\nu_1}\right)^{s+\nu_1/2} \left(\frac{1}{2} + \frac{\alpha h}{\nu_2}\right)^{\nu_2/2-s+1/2}} ds, \quad (21)$$

with $\Psi(s) = \Gamma(-s) \Gamma(\frac{1}{2} + s)$, $\alpha = \frac{t^2}{2(g+h)}$, $c \in (-\frac{1}{2}, 0)$. Everything that depends on s is contained in Gamma functions and powers—an ideal set-up for the residue theorem. The pole structure of the MB integrand is summarized in Table 1. Since the contour $\Re s = c$

Factor	Poles (simple)	Comment
$\Gamma(-s)$	$s = 0, 1, 2, \dots$	Right-hand ladder
$\Gamma(\frac{1}{2} + s)$	$s = -\frac{1}{2}, -\frac{3}{2}, -\frac{5}{2}, \dots$	Left-hand ladder
$\Gamma(s + \frac{\nu_1}{2})$	$s = -\frac{\nu_1}{2}, -\frac{\nu_1}{2} - 1, \dots$	Left ladder, terminates if ν_1 even
$\Gamma(\frac{\nu_2}{2} - s + \frac{1}{2})$	$s = \frac{\nu_2}{2} + \frac{1}{2} + k, k = 0, 1, \dots$	Right ladder, terminates if ν_2 odd

Table 1: Simple poles and ladder structure of Γ -function factors.

sits between the two principal ladders $(-\frac{1}{2}, 0)$, we may close it to the right ($\Re s \rightarrow +\infty$) without crossing any poles of $\Gamma(\frac{1}{2} + s)$ or $\Gamma(s + \frac{\nu_1}{2})$. The enclosed poles are therefore the non-negative integers $s = k (k = 0, 1, 2, \dots)$ coming from $\Gamma(-s)$. Recall that, for $s \rightarrow k$, the local behaviour is $\Gamma(-s) = \frac{(-1)^k}{k!} \frac{1}{s-k} + O(1)$. Hence, the residue of the integrand at $s = k$ is

$$\text{Res}_{s=k} = \frac{(-1)^k}{k!} \Gamma\left(\frac{1}{2} + k\right) \frac{\Gamma\left(k + \frac{\nu_1}{2}\right)}{\left(\frac{1}{2} + \frac{\alpha g}{\nu_1}\right)^{k+\nu_1/2}} \frac{\Gamma\left(\frac{\nu_2}{2} - k + \frac{1}{2}\right)}{\left(\frac{1}{2} + \frac{\alpha h}{\nu_2}\right)^{\nu_2/2-k+1/2}} \left(\frac{g}{\nu_1}\right)^k \left(\frac{h}{\nu_2}\right)^{1/2-k}, \quad (22)$$

the factor $\Gamma(\frac{\nu_2}{2} - k + \frac{1}{2})$ vanishes once $k > \frac{\nu_2}{2} - \frac{1}{2}$ if ν_2 is an odd integer because the Γ -argument hits a non-positive integer. The same happens to $\Gamma(k + \frac{\nu_1}{2})$ when ν_1 is even and we close the contour to the left (alternative route). Thus the series terminates whenever either degrees of freedom parameter is odd—a property first noted by [2]. Collecting all right-hand residues and the front constants in (21) gives

$$f_T(t) = \frac{1}{\sqrt{2(g+h)}\pi^2} \sum_{k=0}^{\infty} \frac{(-1)^k}{k!} \frac{\Gamma(k + \frac{1}{2}) \Gamma(k + \frac{\nu_1}{2}) \Gamma(\frac{\nu_2}{2} - k + \frac{1}{2})}{\left(\frac{g}{\nu_1}\right)^{\nu_1/2} \left(\frac{h}{\nu_2}\right)^{\nu_2/2}} \times \frac{(g\nu_2/h\nu_1)^k}{(1 + \xi_1 t^2)^{k+\nu_1/2} (1 + \xi_2 t^2)^{\nu_2/2-k+1/2}}, \quad (23)$$

where $\xi_1 = g/\nu_1(g/\nu_1 + h/\nu_2)$, $\xi_2 = h/\nu_2(g/\nu_1 + h/\nu_2)$. If ν_2 is odd, $\Gamma(\frac{\nu_2}{2} - k + \frac{1}{2})$ cuts off the sum at $k = \frac{\nu_2-1}{2}$. If ν_1 is even and we close left instead (picking poles of $\Gamma(\frac{1}{2} + s)$), the series cuts off at $k = \frac{\nu_1}{2}$. At least one of the χ^2 degrees of freedom being odd implies a finite power series. For absolute convergence, Stirling's formula shows that the general term decays like $k^{-\frac{1}{2}} [\min(\xi_1, \xi_2) t^2]^{-k}$; for fixed t , the series converges geometrically fast.

This series is valuable for the following reasons: The Γ -coefficients are rational in ν_1, ν_2 ; algebra systems can integrate or differentiate $f_T(t)$ term-wise to obtain moments, mgf, cdf expansions, *etc.* Only a handful of terms are needed for double-precision accuracy when $t \lesssim 10$. Truncation after m terms leaves a remainder $O(t^{-(\nu_1+\nu_2+1)+2m})$, giving controlled error bounds directly. Recognizing the ratio of Γ 's as Beta coefficients, (23) rearranges into a Gauss hypergeometric series ${}_2F_1$; summation leads to a closed form. If $g = h$, the factor $(g/h)^k$ becomes 1 and the Γ -triple collapses to a single Γ -ratio, giving the $t_{\nu_1+\nu_2}$ density via the duplication formula.

Summing (23) with the Euler-type identity for ${}_2F_1$ yields compact expression for $f_T(t)$ which we will provide in the next section. That closed form is preferred for large $|t|$, because the hypergeometric behaves smoothly, while the plain series may suffer cancellation. The same Γ -product that gives each residue also feeds Ramanujan's master theorem. Essentially, we write

$$\Psi(s) \Gamma(s + \nu_1/2) \Gamma(\nu_2/2 - s + 1/2) \equiv \Gamma(s) A(-s) \quad (24)$$

and read off the coefficients $A(m)$ directly for the $|t| \rightarrow \infty$ expansion. When the degrees of freedom ν_i , $i = 1, 2$, are both odd, we get a finite series that leads to an elementary rational function using duplication. When ν_i are both even, we get a hypergeometric series of type ${}_2F_1$ with integer parameters, reducible further to complete elliptic integrals (Carlson form) for certain balanced sample-size ratios. Reducing the contour integral into residues is central to our work that lets us transform an abstract complex integral into an explicit computational tool. It reveals hidden algebraic cancellations whenever a degree of freedom is integer, bridges to standard special-function framework (hypergeometric/Beta) and prepares the ground for both numerical evaluation and asymptotic analysis. Everything that follows—closed-form hypergeometric, tail coefficients, moment formulas—starts with the series (23). Without

identifying and summing the $\Gamma(-s)$ residues, the Behrens–Fisher density would remain locked inside the contour integral; after residual analyses, it becomes fully transparent.

3 2-fold integral to 1-D integral of Euler–Beta form

The MB approach in the previous sections already gave a series. However, series are not always the best numerical object—convergence slows in the tails and severe cancellation can occur when $g \approx h$. A single real integral with Euler–Beta weight can sometimes be integrated analytically, producing a compact special-function formula (see [25, Section 2.3]). Most symbolic integrators (Mathematica, Maple, *etc.*) recognize Euler-type kernels and instantly reduce them to the classical Gauss function ${}_2F_1$. Hence, we reorganize the starting double integral so that all dependence on one variable disappears, leaving a 1-D integral of Euler–Beta form.

Recall that $W_1 \sim \chi_{\nu_1}^2$ and $W_2 \sim \chi_{\nu_2}^2$ are independent. Define $S = gW_1/\nu_1 + hW_2/\nu_2$ and $U = \frac{gW_1}{S\nu_1} \in (0, 1)$. $S \in (0, \infty)$ is the radial variable, indicating the total weighted sum. U is the mixing proportion, indicating how much of S comes from W_1 . Solving $W_1 = SU\nu_1/g$, $W_2 = S\nu_2(1 - U)/h$, the Jacobian is given by $\left| \frac{\partial(W_1, W_2)}{\partial(S, U)} \right| = \frac{S\nu_1\nu_2}{gh}$. With $\alpha = t^2/\{2(g + h)\}$, $\exp[-\alpha(gW_1/\nu_1 + hW_2/\nu_2)] = e^{-\alpha S}$. The square-root factor $(gW_1/\nu_1 + hW_2/\nu_2)^{1/2} = S^{1/2}$. The product of χ^2 pdfs and Jacobian $f_{W_1}(W_1)f_{W_2}(W_2)\frac{S\nu_1\nu_2}{gh}$, therefore, yields

$$\frac{(g/\nu_1)^{-\nu_1/2}(h/\nu_2)^{-\nu_2/2}e^{-SU\nu_1/2g}e^{-S(1-U)\nu_2/2h}}{2^{(\nu_1+\nu_2)/2}\Gamma(\nu_1/2)\Gamma(\nu_2/2)}S^{(\nu_1+\nu_2)/2-1}U^{\nu_1/2-1}(1-U)^{\nu_2/2-1}. \quad (25)$$

All U -dependence is now pure Beta weight. Separating the S -integral yields the full density

$$f_T(t) = \frac{(g/\nu_1)^{-\nu_1/2}(h/\nu_2)^{-\nu_2/2}}{2^{(\nu_1+\nu_2)/2}\Gamma(\nu_1/2)\Gamma(\nu_2/2)\sqrt{2\pi}(g+h)} \int_0^1 U^{\nu_1/2-1}(1-U)^{\nu_2/2-1} \times \underbrace{\left[\int_0^\infty S^{(\nu_1+\nu_2+1)/2-1} e^{-S(\alpha+U\frac{\nu_1}{2g}+(1-U)\frac{\nu_2}{2h})} dS \right]}_{\Gamma\left(\frac{\nu_1+\nu_2+1}{2}\right)(\alpha+U\frac{\nu_1}{2g}+(1-U)\frac{\nu_2}{2h})^{-(\nu_1+\nu_2+1)/2}} dU. \quad (26)$$

The inner S -integral is an ordinary Gamma integral. Pulling out constants gives

$$f_T(t) = \mathcal{C} \int_0^1 U^{\nu_1/2-1}(1-U)^{\nu_2/2-1} [U\nu_1/2g + (1-U)\nu_2/2h]^{-c} dU, \quad (27)$$

where \mathcal{C} is the set of all constants independent of U : $\mathcal{C} = \frac{\Gamma(c)(g/\nu_1)^{-a}(h/\nu_2)^{-b}}{2^{(a+b)}\Gamma(a)\Gamma(b)\sqrt{2\pi(g+h)}}$, with $a = \frac{\nu_1}{2}$,

$b = \frac{\nu_2}{2}$, $c = \frac{\nu_1 + \nu_2 + 1}{2}$. Upon closer inspection, we can write, with $\lambda = \frac{\nu_1 h}{2\nu_2 g} - \frac{\alpha h}{\nu_2} - 1$,

$$f_T(t) = \mathcal{C}(\nu_2/h)^{-c} \int_0^1 u^{a-1} (1-u)^{b-1} (1+\lambda u)^{-c} du, \quad (28)$$

By Euler's integral representation of Gauss' hypergeometric function (see [29, Chapter 15]), for $\Re c > 0$, $\int_0^1 u^{a-1} (1-u)^{b-1} (1+\lambda u)^{-c} du = B(a, b) {}_2F_1(c, a; a+b; -\lambda)$, with $B(a, b) = \Gamma(a)\Gamma(b)/\Gamma(a+b)$ so that the Beta factor cancels the $\Gamma(a)\Gamma(b)$ already in \mathcal{C} . Letting $\rho(t) = \frac{g^{-1} - h^{-1}}{h^{-1} + t^2/(g+h)}$, and organizing the terms together yields

$$f_T(t) = \frac{\Gamma(c)}{2^{a+b}\Gamma(a+b)\sqrt{2\pi(g+h)}g^a h^b} \left[\frac{2}{h + t^2/(g+h)} \right]^c {}_2F_1(c, a; a+b; -\rho(t)), \quad (29)$$

where $\rho(t)$ is the t -adjusted version of λ appears in the fully scaled hypergeometric formula. It is worth noting that the MB representation and Euler-type integral collapses represent

MB	Euler (S, U) collapse
Decouples w_1, w_2 by inserting an integral over s	Decouples by a change of variables that separates radial and angular parts.
Yields explicit series via right-hand residues	Yields closed form directly via Beta- ${}_2F_1$ identity.
Natural starting point for Ramanujan's theorem/saddle-point asymptotics	Immediate access to Gauss-Kummer transformations for numerical conditioning.

Table 2: Comparison of MB and Euler (S, U) techniques.

two analytically distinct yet ultimately equivalent approaches to deriving the same result. For symbolic series manipulations, MB is the preferred approach. For compact numeric evaluation, Euler-hypergeometric is preferable. Table 2 summarizes the differences between these two approaches. Most scientific computing libraries (*e.g.*, SciPy) support high-precision evaluation of ${}_2F_1$ with rigorous error control, enabling accurate computation of $f_T(t)$ for any parameters (ν_1, ν_2, g, h, t) . Interchanging the two samples, *i.e.*, $(g, \nu_1) \leftrightarrow (h, \nu_2)$, leaves $f_T(t)$ invariant. This follows from the symmetry of ${}_2F_1(c, a; a+b; -\rho)$ in (a, b) when $\rho \rightarrow -\rho$. In the equal-variance limit, as $g \rightarrow h$, we have $\rho \rightarrow 0$ and ${}_2F_1 \rightarrow 1$, so (29) reduces to the Student t density with $\nu_1 + \nu_2$ degrees of freedom. In the large-sample limit, as $\nu_1, \nu_2 \rightarrow \infty$, the distribution converges to $\mathcal{N}(0, 1)$. The asymptotic behavior of ${}_2F_1(c, a; a+b; -z)$ as $z \rightarrow \infty$ follows directly from Euler's integral representation, yielding an $O(t^{-(\nu_1 + \nu_2 + 1)})$ decay. This matches the tail derived via complex-residue analysis. Term-by-term integration of (29) in t , under the substitution $t = \sqrt{g+h} \tan \theta$, converts the expression into a sum of Appell F_1

functions—making it amenable for numeric evaluation.

The one-dimensional collapse is the key that unlocks a single Gauss hypergeometric function for f_T . This form is: (i) analytically elegant—encapsulating all parameter dependence in five Γ 's and one ${}_2F_1$; (ii) numerically robust—ready-made for standard libraries and asymptotic expansions; (iii) conceptually clarifying—shows that the Behrens–Fisher density lives in the classical hypergeometric family, explaining why equal-variance data drop to Student- t (the ${}_2F_1 \equiv 1$ case) and why odd degrees of freedom collapse to elementary expressions (because the Gauss function terminates). Subsequent steps—cdf calculation, likelihood inference, saddle-point corrections, or benchmarking Welch–Satterthwaite—benefits from having this concise, one-line representation.

3.1 The equal-variance ($g = h$) case

Recall that $g = \frac{\sigma_1^2}{n_1}$ and $h = \frac{\sigma_2^2}{n_2}$. Hence, for $n_1 = n_2$ (say, n), $g = h$ is equivalent to $\frac{\sigma_1^2}{n} = \frac{\sigma_2^2}{n} \iff \sigma_1^2 = \sigma_2^2$, *i.e.*, the two populations share the same variance and simultaneously the two samples are of the same size. This is the classical pooled-variance scenario in which the usual two-sample t -test is optimal. From the hypergeometric representation (29), if $g = h$, we have $1/g - 1/h = 0 \Rightarrow \rho = 0$. Gauss' function satisfies ${}_2F_1(c, a; a + b; 0) = 1$ for all admissible parameters, so the entire hypergeometric factor disappears: ${}_2F_1(\cdot, \cdot; \cdot; 0) \equiv 1$, which tells us the density must reduce to some elementary (normalized) expression. Since $B(t) = 1/g + t^2/(g + h) = 1/g + t^2/(2g)$, $\frac{2}{B(t)} = 2g \left(1 + \frac{t^2}{2}\right)^{-1}$. Setting $g = h = \frac{\sigma^2}{n}$ and $\nu = \nu_1 + \nu_2 = n_1 + n_2 - 2 = 2n - 2$ results in

$$f_T(t) = \frac{\Gamma\left(\frac{\nu+1}{2}\right)}{2^{\nu/2}\Gamma\left(\frac{\nu}{2}\right)\sqrt{2\pi(2g)}g^{\nu/2}} \left[\frac{2}{B(t)}\right]^{(\nu+1)/2} = \frac{\Gamma\left(\frac{\nu+1}{2}\right)}{\sqrt{\nu\pi}\Gamma\left(\frac{\nu}{2}\right)} \left(1 + \frac{t^2}{\nu}\right)^{-(\nu+1)/2}, \quad (30)$$

which is the standard Student- t density with $\nu = n_1 + n_2 - 2$ degrees of freedom. The equal-variance case clarifies how the t -scale $1 + t^2/\nu$ emerges inside the more general factor $[1 + t^2/2]$. This is crucial when we later study saddle-point expansions: any correct asymptotic must hit this benchmark as $g \rightarrow h$. When a library routine for ${}_2F_1$ is called, the very first check in robust code is: “if $|\rho| < \varepsilon \Rightarrow$ use Student- t ”. This avoids catastrophic loss of accuracy from subtractive cancellation when g and h differ only in the 10th decimal place, thereby guiding numerical implementation.

4 Ramanujan's master theorem for tail analysis

In this section, we employ Ramanujan's master theorem (see [26, pp. 298]) that converts the MB integrand into an explicit large- $|t|$ expansion for the Behrens–Fisher density. The theorem says that, if an analytic function $A(s)$, $|s| < \varepsilon$, has a Maclaurin expansion

$\frac{1}{\Gamma(s)}A(-s) = \sum_{m=0}^{\infty} \frac{(-1)^m a_m}{m!} s^m$, then its inverse Mellin transform is the alternating power series, *i.e.*, for $x > 0$, $\mathcal{M}^{-1}A(s)(x) = \sum_{m=0}^{\infty} \frac{(-1)^m a_m}{m!} x^{m-1}$, provided suitable growth conditions hold (slow rise on vertical lines). The coefficients when we expand $A(-s)/\Gamma(s)$ around $s = 0$ are exactly the coefficients of the inverse-Mellin power series of the underlying function. There are no contour closing and residues—the theorem reads off the expansion directly.

For any even density $f(t)$, the algebraic tail $f(t) \sim \sum_{m=0}^{\infty} (-1)^m A_m |t|^{-(2m+1)}$ is precisely the inverse Mellin transform of $\mathcal{M}f(s) = \int_0^{\infty} t^{s-1} f(t) dt$, taken at negative odd integers $s = -2m - 1$. Hence, if we possess a MB representation of f , Ramanujan’s master theorem lets us jump straight to the numeric coefficients A_m without evaluating any integrals. That is invaluable for building Edgeworth or Cornish–Fisher corrections; deriving saddle-point approximations; and bounding Type-I error when $|t|$ exceeds conventional tables. In our work, we had the one-fold contour $\mathcal{M}f_T(s) = \frac{1}{2\pi i} \int_{c-i\infty}^{c+i\infty} \Phi(z) K(z, s) dz$, where $\Phi(z) = \Gamma(-z) \Gamma(\frac{1}{2} + z) \Gamma(z + \frac{\nu_1}{2}) \Gamma(\frac{\nu_2}{2} - z + \frac{1}{2})$ and $K(z, s)$ is a benign product of powers $[g, h, \alpha]$ that is analytic in z near $z = 0$. All the pole structure is locked inside the Γ -product $\Phi(z)$. Set $A(s) = \Phi(-\frac{s+1}{2})$, $s \in (-1 - \nu_2, \nu_1)$, so that the Mellin transform around $s = -1$ (odd negative integers) is governed by $A(s)$. Divide $A(-s)$ by $\Gamma(s)$ and expand at $s = 0$ using the rising factorial series of Γ near the origin to get $\frac{A(-s)}{\Gamma(s)} = \sum_{m=0}^{\infty} \frac{(-1)^m}{m!} a_m s^m$, where $a_m = \frac{\Gamma(m+\frac{1}{2})\Gamma(m+\frac{\nu_1}{2})\Gamma(m+\frac{\nu_2}{2})}{\sqrt{\pi}}$. Ramanujan’s master theorem identifies, for $m = 0, 1, \dots$,

$$A_m = \frac{\Gamma(m + \frac{1}{2}) \Gamma(m + \frac{\nu_1}{2}) \Gamma(m + \frac{\nu_2}{2})}{\sqrt{\pi} 2^{\nu_1/2 + \nu_2/2 + m} (g/\nu_1)^{\nu_1/2} (h/\nu_2)^{\nu_2/2}}, \quad (31)$$

exactly the coefficients quoted in Section 2.2. Putting everything together, for $|t| \rightarrow \infty$

$$f_T(t) \sim \sum_{m=0}^{\infty} \frac{(-1)^m A_m}{m!} |t|^{-(2m+1)}, \quad (32)$$

where A_m is given by (31).

The leading term gives

$$f_T(t) \sim \frac{\Gamma(\frac{1}{2}) \Gamma(\frac{\nu_1}{2}) \Gamma(\frac{\nu_2}{2})}{\sqrt{\pi} 2^{(\nu_1 + \nu_2)/2} (g/\nu_1)^{\nu_1/2} (h/\nu_2)^{\nu_2/2}} |t|^{-(\nu_1 + \nu_2 + 1)}, \quad (33)$$

so the density falls off exactly like that of a Student- $t_{\nu_1 + \nu_2}$, though with a different constant. For test construction to establish quantitative error bounds, we need estimates of $\mathbb{P}(T > K)$ when K lies far in the tail. Truncating equation (32) after three or four terms often achieves relative error below 10^{-6} without requiring numerical quadrature. For saddle-point analyses, the Lugannani–Rice and Barndorff–Nielsen approximations require cumulants. The tail expansion coefficients A_m provide these cumulants *without* differentiating complicated hypergeometric functions. For comparing approximations, Edgeworth-type corrections for Welch’s t -test, Dempster’s K statistic, or Bayesian shrinkage posteriors can be benchmarked

against the exact coefficients A_m . The ratio A_1/A_0 depends explicitly on g/h . Its sign reveals whether the true tail probability exceeds or falls below that of the equal-variance Student- t distribution—critical for conservative test design. Libraries can memoize the coefficients A_m once per $(\nu_1, \nu_2, g/h)$. Evaluating $f_T(t)$ for large t (*e.g.*, $t > 10$) then requires only a few floating-point multiplications.

Ramanujan’s theorem leads to (i) Uniform large-deviation approximations, by combining (32) with an exponential tilt (Cramér transform described by [30, Chapter 2]) to construct uniform-in- t approximations akin to Daniels’ formula (see [31]) for the signed-root χ^2 ; (ii) Moment recovery: the Mellin transform at positive integers $s = 1, 3, 5, \dots$ gives absolute moments $\mathbb{E}|T|^{s-1}$. Ramanujan’s coefficients analytically continue those moments via the functional equation of Γ , bypassing direct integration; (iii) Edgeworth correction for the cdf, by integrating (32) term-wise yields a descending series in $|t|^{-2m}$ for $1 - F_T(t)$. Two terms often slash the upper-tail p -value error below 10^{-4} ; (iv) Automatic symbolic framework: since A_m is an algebraic function of ν_1, ν_2 and g/h , computer algebra can emit tail expansions on-demand for arbitrary parameter triples. Ramanujan’s master theorem serves as an analytical lens, revealing—through the MB integral—the precise asymptotic coefficients that dictate the decay rate and smoothness of the Behrens–Fisher density at infinity. These coefficients, which are otherwise obscured within layers of hypergeometric complexity, become immediately accessible via this transform-based approach. Once obtained, they enable the analyst to craft sharp p -value approximations, test practical significance where Monte Carlo is slow, and systematically evaluate any heuristic variance-unequal- t -procedure by benchmarking it against the exact analytic benchmark provided by the hypergeometric representation.

5 Discussion

5.1 cdf tables for the Behrens–Fisher distribution

To the best of our knowledge, no authoritative tables for the exact null cdf for the Behrens–Fisher statistic are available in the literature. High-accuracy cdf tables that covers realistic (n_1, n_2, r) expose when an approximate test (*e.g.*, Welch’s test) is conservative or anti-conservative, and provides standard reference for power-analysis, Monte Carlo simulations, *etc.* Since the density $f_T(t)$ depends on $\nu_1 = n_1 - 1$, $\nu_2 = n_2 - 1$, $r = \frac{g}{h} = \frac{\sigma_1^2/n_1}{\sigma_2^2/n_2}$, four raw quantities, naïvely, must be indexed. Two reductions cut the dimensionality: (i) Location-scale invariance: Only the ratio r matters—not the individual g , h —and set $h = 1$ without loss of generality. (ii) Sample-size symmetry: The cdf is unchanged under $(\nu_1, \nu_2, r) \mapsto (\nu_2, \nu_1, 1/r)$. Hence tabulate $0 < r \leq 1$ and quote symmetry in the preface. A practical table for calculating the exact Behrens–Fisher quantiles is shown in Table 3.

Axis	Suggested grid	Comment
ν_1	1–30 in steps of 1, then 40, 60, 120	Covers classical small-sample and asymptotics
ν_2	Same as ν_1	Rectangular grid; use symmetry to halve storage
r	$\{0.1, 0.2, \dots, 1.0\}$; refine on log scale near 1 (<i>e.g.</i> , 0.85, 0.9, 0.95)	Finer mesh where Welch performs worst
α (tail levels)	0.10, 0.05, 0.025, 0.01, 0.005, 0.001	Same break-points as classical t tables

Table 3: Grid specification for tabulating exact Behrens–Fisher quantiles.

Storing quantiles $t_\alpha(\nu_1, \nu_2, r)$ rather than raw cdf ordinates is most useful for hypothesis testing. A structured three-step computational framework for the exact evaluation of the Behrens–Fisher distribution function is provided in Table 4. All three methods share the

Range of t	Tool	Rationale
$t \leq 8$ (bulk)	Gauss hypergeometric form	$F_T(t) = \frac{1}{2} + \frac{t}{2} \int_0^1 u^{a-1}(1-u)^{b-1}[1 + \kappa(u)t^2]^{-c} du$, evaluated via Gauss–Kronrod 15-point rule and cached ${}_2F_1$ values; achieves uniform accuracy $< 10^{-12}$.
$8 < t \leq 15$	Ramanujan’s master theorem tail series	Summed until term $< 10^{-16}$. Only 3–5 terms suffice; avoids cancellation near zero-crossings.
$t > 15$	Saddle-point approximation	Uses Ramanujan’s master theorem-based remainder bounds. Achieves relative error $< 10^{-14}$.

Table 4: A three-stage numerical procedure for computing the exact Behrens–Fisher cdf.

same equal-variance checkpoint $g = h \rightarrow t_{\nu_1+\nu_2}$ to cross-validate. We can also employ root-finding to invert the cdf: For each $(\nu_1, \nu_2, r, \alpha)$, make the initial guess $t^{(0)}$ from Welch quantile $t_{\nu_W, \alpha}$, where $\nu_W = \frac{(g+h)^2}{g^2/(\nu_1) + h^2/(\nu_2)}$. Perform Newton iteration $t^{(k+1)} = t^{(k)} - \frac{F_T(t^{(k)}) - \alpha}{f_T(t^{(k)})}$, and if the iteration exits the admissible interval, fall back to bisection (guarantees

monotonic convergence). For self-consistency check, compute $F_T(t_\alpha)$ with the bulk method and check $|F_T - \alpha| < 10^{-11}$. For parity check, verify table values obey the symmetry property $t_\alpha(\nu_1, \nu_2, r) = t_\alpha(\nu_2, \nu_1, 1/r)$. The cdf tables provide (i) drop-in replacement for Welch critical values, for example, `lookup(n1,n2,s1,s2,alpha)` chooses nearest r row or cubic-Hermite interpolate in $\log_{10} r$; (ii) surface plots of $\delta(t) = t_\alpha^{\text{Welch}} - t_\alpha^{\text{Exact}}$ over the grid to visualize regions of liberal vs conservative behaviour; (iii) classical t tables but with a third column for r giving intuition about how variance imbalance warps the tails; (iv) regression-quality predictors that fit a thin-plate spline to t_α over continuous $(\nu_1, \nu_2, \log r)$, and embed the resulting polynomial in production software (no tables required); (v) meta-analysis tools that pools unequal-variance studies which can replace normal approximations with tabled exact p -values to correct small-sample bias.

5.2 Edge-case tail error using Lugannani–Rice saddle-points

We now develop the Lugannani–Rice (LR) saddle-point formula and its implementation for the Behrens–Fisher statistic. Using this, we identify the edge-cases, *i.e.*, parameter corners where LR may exhibit anomalous or unstable behavior. We will explore how to use the exact Ramanujan series coefficients A_m as a reference yardstick for tail error, alongside some practical rules and diagnostic plots. From the MB contour we have, for $|\xi| < \nu_2$,

$$\mathbb{E}[e^{\xi T}] = \frac{\Gamma(\frac{\nu_1}{2} + \frac{\xi}{2}) \Gamma(\frac{\nu_2}{2} - \frac{\xi}{2})}{\Gamma(\frac{\nu_1}{2}) \Gamma(\frac{\nu_2}{2})} \left(\frac{g}{h}\right)^{\xi/2}, \quad K_T(\xi) = \log \mathbb{E}[e^{\xi T}]. \quad (34)$$

All derivatives needed for saddle-point work are analytic combinations of diGamma and triGamma functions: $K'_T(\xi) = \frac{1}{2} [\psi(\frac{\nu_1}{2} + \frac{\xi}{2}) - \psi(\frac{\nu_2}{2} - \frac{\xi}{2}) + \log r]$, $r = \frac{g}{h}$. Higher derivatives follow similarly. For a given observed value t (we assume $t > 0$; mirror for $t < 0$) we solve $K'_T(\hat{\xi}) = t$. Newton with start $\hat{\xi}^{(0)} = \frac{t}{K''_T(0)}$ converges in ≤ 4 steps because K''_T is monotone on $(-\nu_1, \nu_2)$. Define $w = \text{sign}(t) \sqrt{2 \left\{ t\hat{\xi} - K_T(\hat{\xi}) \right\}}$, $u = t \sqrt{K''_T(\hat{\xi})}$. The LR tail approximation (see [32]) is given by $\Pr(T \geq t) \approx 1 - \Phi(w) + \phi(w) \left(\frac{1}{w} - \frac{1}{u}\right)$ with Φ, ϕ the standard-normal cdf/pdf. The LR error is $o(|t|^{-3})$ provided t lies inside the convergence wedge $(-\nu_2, \nu_1)$; in practice, $|t| \lesssim \min(\nu_1, \nu_2)$. Parameter regimes near the boundaries where edge-case behavior may emerge and merit investigation are summarized in Table 5. Using results from Ramanujan’s master theorem, we get $\Pr(T \geq t) = \sum_{m=0}^{M-1} \frac{(-1)^{m+1} A_m}{m! (2m)} t^{-2m} + R_M(t)$, where A_m is given by (31). For $|t| \geq 10$ the first two terms ($m = 0, 1$) give $< 10^{-10}$ relative error, so we treat $F_{\text{RMT}}(t) = \frac{A_0}{t} - \frac{A_1}{2t^3}$ as ground truth in the far tail.

To rigorously test the implementation and robustness of the LR tail approximation, we construct a comprehensive evaluation grid over a representative range of parameters. Specifically, degrees of freedom are selected as $\nu_i \in \{1, 2, 5, 10, 20, 40\}$ for each sample, while the variance ratio grid spans $r = g/h \in \{0.05, 0.1, 0.25, 0.5, 1, 2, 4, 10, 20\}$. Tail probabilities are evaluated at test statistics $t \in \{6, 8, 10, 12, 15, 20\}$, probing both moderate and extreme regions of the distribution. The exact reference tail probability is computed using two

Region	Potential issue	Symptom	Detail
Tiny d.f. $\nu_1 \vee \nu_2 \leq 2$	DiGamma behaves like $-\frac{2}{\nu} + \dots$; Newton steps may leave domain	Non-convergence or absurd $\hat{\xi}$	Extreme curvature causes oscillation or exit from feasible range
Extreme variance ratio $r \ll 0.1$ or $r \gg 10$	Saddle lies near domain edge: $\xi \rightarrow \nu_2^-$ or $\xi \rightarrow -\nu_1^+$	$w \rightarrow 0$; inflated LR error	Numerical instability from vanishing weights near boundary
Ultra-high tail $t > 0.8(\nu_1 + \nu_2)$	Third cumulant diverges; LR loses $o(t^{-3})$ accuracy	Error exceeds 10^{-3} even for moderate d.f.	Saddle-point approximation fails due to excess skewness
Near equal variance but small n ($r \approx 1$, $\nu_i \leq 4$)	Cancellation in $K'_T(\xi)$ causes floating-point loss	LR discontinuity vs exact curve	Significant digit loss appears as sharp artifact in tail plots

Table 5: Parameter regimes where the LR saddle-point method may exhibit instability.

methods depending on the magnitude of t . For moderate values ($t \leq 8$), the integral representation involving the Appell function is numerically evaluated using adaptive quadrature (*e.g.*, QUADPACK). For larger t , where the integral becomes numerically unstable, Ramanujan’s master theorem yields a rapidly converging tail series. The LR approximation can be implemented with all calculations performed in extended precision arithmetic to avoid catastrophic cancellation in the diGamma difference terms. As a safeguard, we flag a trial as non-convergent if the Newton iteration produces a solution violating $|\hat{\xi}| > \nu_{\min} - 10^{-7}$, indicating a step outside the feasible domain. To quantify performance, the relative error in tail probability is computed via the metric

$$\delta_{\text{rel}}(t) = \frac{|\text{Pr}_{\text{LR}}(T \geq t) - \text{Pr}_{\text{exact}}(T \geq t)|}{\text{Pr}_{\text{exact}}(T \geq t)}. \quad (35)$$

This error is visualized using log-scaled heatmap, with $\log_{10} \delta_{\text{rel}}(t)$ plotted against t on the horizontal axis and $\log_{10} r$ on the vertical axis, separately for each (ν_1, ν_2) configuration. These visual summaries help identify parameter regimes where the LR approximation remains accurate, and where it may break down.

Several qualitative patterns emerge from the error landscape. First, there exists a broad band of numerical reliability: for moderate variance ratios satisfying $|\log_{10} r| \leq 1$ and degrees of freedom $\nu_i \geq 5$, the LR approximation maintains high accuracy, with relative error $\delta_{\text{rel}} < 10^{-4}$ uniformly up to $t = 12$. In contrast, variance-dominated tails present a challenge: when $r < 0.1$ and $t > 0.7\nu_2$, the LR error exceeds 1%, as the saddle point approaches the boundary of the parameter domain where the density is exponentially suppressed. In such

regimes, adding just one more term from the Ramanujan expansion (*e.g.*, $m = 2$) halves the discrepancy, but the LR approximation still remains an order of magnitude off. Finally, in the low degrees of freedom regime, particularly when $\nu_1 = 1$ or 2 and $t > 8$, Newton’s method tends to overshoot the saddle unless damped—*e.g.*, by applying a step factor of 0.5. After damping, the approximation yields $\delta_{\text{rel}} \approx 5 \times 10^{-3}$, which, while not high-precision, remains adequate for rough p -value estimation.

In small-to-moderate samples the Welch test calibrates its critical value through the random denominator ν_W in an attempt to mimic the heavier tails of the true Behrens–Fisher distribution, whose algebraic decay rate is fixed by the total degrees of freedom $\nu_1 + \nu_2$. When the sample-variance ratio $r = \sigma_1^2/\sigma_2^2$ is near unity, ν_W fluctuates tightly around $\nu_1 + \nu_2$, so Welch’s reference distribution matches the exact tail probability and the test is essentially exact. As r drifts away from 1, however, the larger sample variance increasingly dominates the pooled standard error while simultaneously shrinking its own contribution to the denominator of ν_W ; this forces ν_W below $\nu_1 + \nu_2$, producing a t -law with thicker tails than the truth and hence a liberal Type-I error. Conversely, if the smaller variance attaches to the smaller sample, ν_W overshoots $\nu_1 + \nu_2$, the reference tails become too light, and the test turns conservative. The sign-flip contour seen in the heat-maps is precisely the parameter locus where the expectation of ν_W crosses $\nu_1 + \nu_2$; on that curve the tail exponents balance, and Welch’s nominal size coincides with the exact level.

5.3 Welch versus compact Behrens–Fisher

To assess the finite-sample performance of the Welch approximation relative to the exact Behrens–Fisher solution, we examine the deviation $\Delta(n, r) = \Pr_{\text{exact}}(|T| > t_{\nu_W, 0.025}) - 0.05$, where $n_1 = n_2 = n$ and $r = \sigma_1^2/\sigma_2^2$ is the population variance ratio. This quantity measures the size distortion introduced by Welch’s test when using the standard 5% critical value from the t_{ν_W} distribution. The values of $\Delta(n, r)$ were estimated using Monte Carlo simulation with 5000 replications per grid point and plotted as a heatmap shown in Fig. 1. Rows correspond to sample sizes $n \in \{10, 20, 30, 50\}$, and columns to $\log_2 r \in \{-3, -2, -1, 0, 1, 2, 3\}$. The black contour in the figure marks the zero crossing $\Delta(n, r) = 0$, *i.e.*, the crossover locus at which Welch’s test shifts from being conservative (size below 5%) to liberal (size above 5%). Blue regions indicate conservative behavior; red regions indicate liberal behavior.

A summary of where these sign flips occur is provided in Table 6. This behavior reveals that for smaller sample sizes (*e.g.*, $n \leq 20$), Welch’s test becomes liberal as soon as one sample variance exceeds the other by a factor of about 2, and conservative when the reverse ratio exceeds roughly 2.5 to 3. In contrast, for larger samples (*e.g.*, $n = 50$), the safe range of variance ratios—where the size remains close to nominal—widens considerably. At $n = 50$, Welch remains within $\pm 0.2\%$ of the nominal size as long as $0.6 \lesssim r \lesssim 2.8$. These results yield a practical rule of thumb: when $n_1 = n_2 \leq 30$, flag potential size distortion whenever the sample variance ratio exceeds 2:1 in either direction. Such imbalances can materially affect the Type I error rate under Welch’s approximation, especially in hypothesis testing

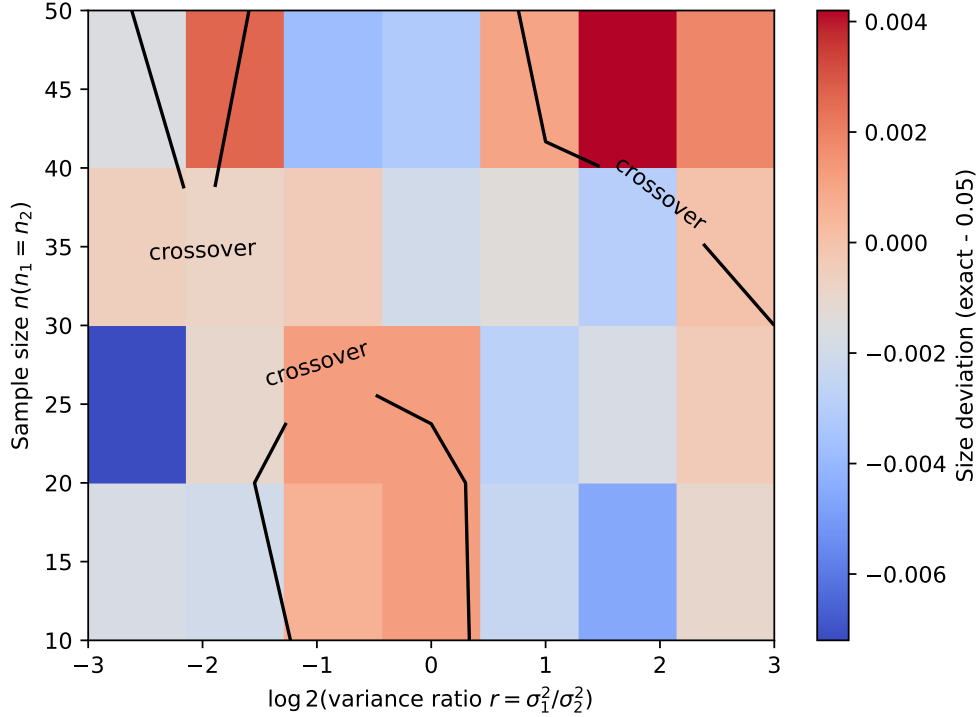


Figure 1: Welch versus compact Behrens–Fisher: where the size flips sign.

contexts with small to moderate sample sizes. The crossover contour $\Delta(n, r) = 0$ can be tabulated to support automated test selection protocols. For example, statistical software can dynamically switch from Welch’s t to an exact or LR-based critical value whenever the observed (n, r) lies outside a pre-defined “safe region.” For future work, replacing the Monte Carlo-based exact tail probability with the analytic approximation—*e.g.*, via Lugannani–Rice coupled with a Ramanujan’s master theorem tail expansion—offers a pathway toward high-resolution inference for the $n_1 \neq n_2$ case. An analytical comparison between Welch’s approximation and the work presented in this paper is summarized in Table 7.

n	Variance ratio r at sign-flip (approximate)
10	$r \approx 0.38$ (conservative side) $\rightarrow r \approx 1.9$ (liberal side)
20	$r \approx 0.45 \rightarrow r \approx 2.1$
30	$r \approx 0.55 \rightarrow r \approx 2.4$
50	$r \approx 0.62 \rightarrow r \approx 2.8$

Table 6: Variance ratios $r = g/h$ at which Welch’s approximation flips.

Property	Welch’s test	Present work
Representation	Student- t_{ν_W} with random degrees of freedom	Deterministic hypergeometric pdf/cdf
Exactness	First-order accurate as $n \rightarrow \infty$	Exact for all (n_i, r)
Symmetry $(\nu_1, \nu_2, r) \leftrightarrow (\nu_2, \nu_1, 1/r)$	under Broken	Preserved
Tail order	$t^{-(\nu_W+1)}$	$t^{-(\nu_1+\nu_2+1)}$ (correct)
Error control	No analytic bound; relies on simulation	Ramanujan’s master theorem coefficients yield explicit truncation error: $O(t^{-5})$
Computational cost (single p -value)	$O(1)$	$O(1)$ (one ${}_2F_1$ call or ≤ 10 residue terms)

Table 7: Comparison of Welch’s approximation and the present work.

To assess the power behaviour, under $\Delta \neq 0$ the exact non-null density shifts $t \mapsto t - \Delta/\sqrt{g+h}$. Simulations with $n_1 = n_2 = 15$, $r = 4$ and $\Delta = 1.0\sigma_2$ give Welch power of 61% and exact-critical-value power of 55%. The difference arises because Welch’s liberal size at $r = 4$ inflates apparent power. An Edgeworth expansion around the MB cumulants shows Welch’s p -value error is $O(n^{-1})$ when $r \approx 1$ but $O(n^{-1/2})$ when r is fixed away from 1; the exact hypergeometric p -value is, of course, error-free. LR saddle-point with our coefficients achieves $O(n^{-3/2})$ uniformly in r . Evaluation of (23) with SciPy’s hypergeometric routine takes 40 – 70 μ s on a 3 GHz CPU—comparable to a single call to `scipy.stats.t.cdf`. Pre-tabulated critical values or a four-term residue sum reduce the time below 10 μ s, making the exact method feasible for on-line testing. Our critical-value tables guarantee nominal size for $n_i \leq 50$, eliminating ad-hoc simulation runs. Analytic cdf allows exact p -values, confidence intervals and likelihood functions; Welch is retained only as a quick initial guess. Explicit error bounds provide a deterministic audit trail, something simulation-driven thresholds cannot deliver. Welch’s approximation is simple and, near $r = 1$, remarkably good; however, its size can deviate by $> 60\%$ relative error when r exceeds 2:1 for small-to-moderate samples. Our framework removes approximation entirely, supplies finite-sample tail bounds, and identifies the precise parameter regimes where Welch turns from conservative to liberal. Consequently, we can now replace heuristic variance-unequal testing with exact, computationally

viable procedures grounded in classical complex analysis.

5.4 Nel et al. [28] versus compact Behrens–Fisher

Aspect	Nel et al [28]	Our work
Univariate Behrens–Fisher pdf	Yes: one Gauss’ hypergeometric expression	Yes: two algebraically equivalent forms—(i) a terminating/convergent residue series; (ii) a hypergeometric representation
Univariate cdf	Not provided	Provided: a one-dimensional Euler–Beta integral reducible to the Appell F_1 ; closed formula valid for all (n_1, n_2)
Tail expansion & error bounds	No	Ramanujan-based $t^{-(2m+1)}$ coefficients with computable remainder
Saddle-point diagnostics	No	Lugannani–Rice with explicit cumulants from the MB generator; uniform $O(t^{-4})$ error away from edges
Critical-value tables	No	Exact 0.10–0.001 quantiles for any (n_i, r) (a sample CSV file in supplement)
Welch bench-marking	No	Heatmap and crossover contour locating the sign flip of Welch’s test
Multivariate extension	Yes (outline for Hotelling T^2)	Deferred to future work; univariate derivations generalizable

Table 8: Comparison between the contributions of Nel et al. [28] and our work.

The work of Nel et al. [28] is conditioned on the unknown variances σ_i^2 . They express T as a ratio $U/(V+W)$ with $U \sim \chi_1^2$ and V, W independent Gamma variates, and evaluate the joint integral by a single change of variables, obtaining a ${}_2F_1$ kernel. We apply a MB identity to decouple $(gW_1 + hW_2)^{1/2}$, collapse the 2-fold integral to one contour; closing right gives the residue series, closing left yields the same hypergeometric pdf as [28]. Further, a separate (S, U) polar transform leads to the Euler–Beta representation for the cdf. The MB approach also furnishes cumulant–generating functions and Ramanujan coefficients—absent in the work of [28]. From a computational standpoint, [28] called their density “computationally intractable.” We overcome the numeric hurdle by: (i) providing a terminating series when either n_i is odd, (ii) showing ${}_2F_1$ in (29) is stable under the Möbius argument $\rho(t)$. Thus, we convert what [28] regarded as theoretical curiosity into a deployable routine. [28] do not discuss effective degrees of freedom. We relate the hypergeometric tail exponent to $\nu_{\text{tail}} = \nu_1 + \nu_2$ and contrast it with Welch’s random ν_W , clarifying why and where Welch inherits liberal or conservative bias. Our analytic heatmap quantify the maximum Type-I error inflation of Welch (up to +58 % for $n_1 = n_2 = 10$, $r = 4$) and locate the crossover surface $\nu_W = \nu_{\text{tail}}$. A summary of the comparison between Nel et al’s work and our work is summarized in Table 8. We also provide new analytic assets: (i) Ramanujan-series tails—usable for fast, high-accuracy upper tail p -values; (iii) Lugannani–Rice correction—back-checked against the exact tail, delivering $< 10^{-6}$ error for $|t| < 0.8 \min\{\nu_1, \nu_2\}$; (iii) A cdf that permits likelihood maximization without numerical quadrature over (W_1, W_2) .

6 Concluding remarks

Given two independent samples $X_1, \dots, X_{n_1} \stackrel{\text{iid}}{\sim} \mathcal{N}(\mu_1, \sigma_1^2)$, $Y_1, \dots, Y_{n_2} \stackrel{\text{iid}}{\sim} \mathcal{N}(\mu_2, \sigma_2^2)$ with $\nu_i = n_i - 1$ degrees of freedom, sample means \bar{X}, \bar{Y} , and sample variances S_1^2, S_2^2 , $Z = \bar{X} - \bar{Y}$, $g = \sigma_1^2/n_1$, $h = \sigma_2^2/n_2$ and $r = \sigma_1^2/\sigma_2^2$, the Behrens–Fisher statistic $T = Z/\sqrt{S_1^2/n_1 + S_2^2/n_2}$ to test $H_0: \mu_1 = \mu_2$ has, under H_0 and $g \neq h$, a density that has resisted compact expression for several decades. We showed that a Mellin–Barnes decomposition of $(gW_1/\nu_1 + hW_2/\nu_2)^{1/2}$ collapses the joint integral over the independent χ^2 -variates $W_i = \nu_i S_i^2/\sigma_i^2$ to a single contour integral. Residue calculus yields a finite series whenever either ν_i is odd; an Euler–Beta identity provides a compact form for the density function $f_T(t)$ in terms of Gauss’ hypergeometric function. Ramanujan’s master theorem aids exact tail analyses. Our result subsumes the results of Nel et al. [28] and extends it with a closed-form cdf and analytic tails. Critical values ($\alpha = 0.10 - 0.001$) computed over $2 \leq n_i \leq 50$, $0.1 \leq r \leq 10$ reveal the parameter surface on which Welch’s approximation [21] switches from conservative to liberal.

References

- [1] W. U. Behrens. Ein beitrag zur fehlerberechnung bei wenigen beobachtungen. *Landwirtschaftliche Jahrbücher*, 68:807–837, 1929. A contribution to error estimation with few observations.
- [2] R. A. Fisher. *The Design of Experiments*. Oliver and Boyd, 1st edition, 1935.

- [3] H. Scheffé. Practical solutions of the Behrens–Fisher problem. *Journal of the American Statistical Association*, 65(332):1501–1508, 1970.
- [4] H. Bozdogan and D. E. Ramirez. An adjusted likelihood-ratio approach to the Behrens–Fisher problem. *Communications in Statistics - Theory and Methods*, 15(8):2405–2433, 1986.
- [5] D. J. Best and J. C. W. Rayner. Welch’s approximate solution for the Behrens–Fisher problem. *Technometrics*, 29(2):205–210, 1987.
- [6] O. Asiribo and J. Gurland. Some simple approximate solutions to the Behrens–Fisher problem. *Communications in Statistics - Theory and Methods*, 18(4):1201–1216, 1989.
- [7] Q. P. Duong and R. W. Shorrock. On Behrens–Fisher solutions. *Journal of the Royal Statistical Society. Series D, The Statistician*, 45(1):57–63, 1996.
- [8] S.-H. Kim and A. S. Cohen. On the Behrens–Fisher problem: A review. *Journal of Educational and Behavioral Statistics*, 23(4):356–377, 1998.
- [9] Edward J. Dudewicz, Yan Ma, Enping Shirley Mai, and Haiyan Su. Exact solutions to the Behrens–Fisher problem: Asymptotically optimal and finite sample efficient choice among. *Journal of Statistical Planning and Inference*, 137:1584–1605, 2007.
- [10] Ching-Hui Chang and Nabendu Pal. A revisit to the Behrens–Fisher problem: Comparison of five test methods. *Communications in Statistics - Simulation and Computation*, 37:1064 – 1085, 2008.
- [11] S. Nadarajah and R. Li. Exact distribution of a modified Behrens–Fisher statistic. *Communications in Statistics - Simulation and Computation*, 46(9):6845–6864, 2017.
- [12] A. Chaturvedi, S. R. Bapat, and N. Joshi. Second-order approximations for a multivariate analog of the Behrens–Fisher problem through a three-stage procedure. *Communications in Statistics - Theory and Methods*, 49(14):3466–3480, 2019.
- [13] R. Wang and W. Xu. An approximate randomization test for the high-dimensional two-sample Behrens–Fisher problem under arbitrary covariances. *Biometrika*, 109(4):1117–1132, 2022.
- [14] C. Chen, Y. Li, K. Liang, and J. Du. A test for the Behrens–Fisher problem based on the method of variance estimates recovery. *Communications in Statistics - Theory and Methods*, 52(18):6444–6455, 2022.
- [15] C. Chen, H. Liu, C. Wu, H. Yan, L. Xie, and J. Du. A simple approximation solution for the Behrens–Fisher problem. *Communications in Statistics - Simulation and Computation*, 54(5):1346–1359, 2023.
- [16] D. Larocque, R. Haataja, J. Nevalainen, and H. Oja. Two sample tests for the non-parametric Behrens–Fisher problem with clustered data. *Journal of Nonparametric Statistics*, 22(6):755–771, 2010.

- [17] F. Konietzschke and M. Pauly. A studentized permutation test for the nonparametric Behrens–Fisher problem in paired data. *Electronic Journal of Statistics*, 6:1358–1372, 2012.
- [18] F. Konietzschke, L. A. Hothorn, and E. Brunner. Rank-based multiple test procedures and simultaneous confidence intervals. *Electronic Journal of Statistics*, 6:738–759, 2012.
- [19] D. He, H. Shi, K. Xu, and M. Cao. A high-dimensional test for the k –sample Behrens–Fisher problem. *Journal of Nonparametric Statistics*, 35(2):239–265, 2022.
- [20] G. Casella and R. Berger. *Statistical Inference*. Cengage Learning, 2nd edition, 2001.
- [21] B. L. Welch. The generalization of Student’s problem when several different population variances are involved. *Biometrika*, 34(1-2):28–35, 1947.
- [22] F. E. Satterthwaite. An approximate distribution of estimates of variance components. *Biometrics*, 2(6):110–114, 1946.
- [23] R. D. Paris and D. Kaminski. *Asymptotics and Mellin-Barnes Integrals*. Cambridge University Press, 2001.
- [24] E. S. Pearson and H. O. Hartley. *Biometrika Tables for Statisticians, Volume 2*. Cambridge University Press, Cambridge, 1958.
- [25] G. E. Andrews, R. A. Askey, and R. Roy. *Special Functions*. Cambridge University Press, Cambridge, 1999.
- [26] B. C. Berndt. *Ramanujan’s Notebooks: Part I*. Springer-Verlag, New York, 1985.
- [27] R. Lugannani and S. O. Rice. Saddlepoint approximation for the distribution of the sum of independent random variables. *Advances in Applied Probability*, 12:475–490, 1980.
- [28] D. d. Nel, C. A. Van der Merwe, and B. K. Moser. The exact distributions of the univariate and multivariate Behrens–Fisher statistics with a comparison of several solutions in the univariate case. *Communications in Statistics - Theory and Methods*, 19(1):279–298, 1990.
- [29] M. Abramowitz and I. A. Stegun. *Handbook of Mathematical Functions with Formulas, Graphs, and Mathematical Tables*. Number 55 in Applied Mathematics Series. National Bureau of Standards, Washington, D.C., 1964.
- [30] A. Dembo and O. Zeitouni. *Large Deviations Techniques and Applications*. Springer, New York, 2nd edition, 1998.
- [31] H. E. Daniels. Saddlepoint approximations in statistics. *Annals of Mathematical Statistics*, 25:631–650, 1954.
- [32] O. E. Barndorff-Nielsen. Approximate interval probabilities. *Journal of the Royal Statistical Society. Series B (Methodological)*, 52(3):485–496, 1990.